Dissecting the pathogenic mechanisms of mutations in the pore region of the human cone photoreceptor cyclic nucleotide-gated channel

Katja Koeppen, Peggy Reuter, Thomas Ladewig, Susanne Kohl, Britta Baumann, Samuel Gregory Jacobson, Astrid Plomp, Christian P Hamel, Andreas Janecke, Bernd Wissinger

▶ **To cite this version:**

Katja Koeppen, Peggy Reuter, Thomas Ladewig, Susanne Kohl, Britta Baumann, et al.. Dissecting the pathogenic mechanisms of mutations in the pore region of the human cone photoreceptor cyclic nucleotide-gated channel. Human Mutation, 2010, 31 (7), pp.830. 10.1002/humu.21283 . hal-00552398

HAL Id: hal-00552398
https://hal.science/hal-00552398

Submitted on 6 Jan 2011

HAL is a multi-disciplinary open access archive for the deposit and dissemination of scientific research documents, whether they are published or not. The documents may come from teaching and research institutions in France or abroad, or from public or private research centers.

L'archive ouverte pluridisciplinaire **HAL**, est destinée au dépôt et à la diffusion de documents scientifiques de niveau recherche, publiés ou non, émanant des établissements d'enseignement et de recherche français ou étrangers, des laboratoires publics ou privés.

Human Mutation

Dissecting the pathogenic mechanisms of mutations in the pore region of the human cone photoreceptor cyclic nucleotide-gated channel

For Review Only

Journal:	*Human Mutation*
Manuscript ID:	humu-2009-0276.R1
Wiley - Manuscript type:	Research Article
Date Submitted by the Author:	07-Apr-2010
Complete List of Authors:	Koeppen, Katja; Institute for Ophthalmic Research, Molecular Genetics Laboratory; Dartmouth Medical School, Department of Physiology Reuter, Peggy; Institute for Ophthalmic Research, Molecular Genetics Lab Ladewig, Thomas; Institute for Ophthalmic Research, Molecular Genetics Lab Kohl, Susanne; Institute for Ophthalmic Research, Molecular Genetics Lab Baumann, Britta; Institute for Ophthalmic Research, Molecular Genetics Lab Jacobson, Samuel; Scheie Eye Institute, Opththalmology Plomp, Astrid; Netherlands Institute for Neuroscience, Department of Clinical and Molecular Ophthalmogenetics Hamel, Christian; Institute for Neurosciences of Montpellier, Hôpital Saint Eloi Janecke, Andreas; Innsbruck Medical University, Division of Clinical Genetics Wissinger, Bernd; Molecular Genetics Laboratory, Institue for Ophthalmic Research, Centre for Ophthalmology
Key Words:	achromatopsia, CNG channel, CNGA3, pore mutation

scholarONE™ Manuscript Central

Dissecting the pathogenic mechanisms of mutations in the pore region of the human cone photoreceptor cyclic nucleotide-gated channel

Katja Koeppen[1,§*], Peggy Reuter[1*], Thomas Ladewig[1], Susanne Kohl[1], Britta Baumann[1], Samuel G. Jacobson[2], Astrid S. Plomp[3], Christian P. Hamel[4], Andreas R. Janecke[5] and Bernd Wissinger[1]

[1]*Molecular Genetics Laboratory, Institute for Ophthalmic Research, Tuebingen, Germany*

[2]*Scheie Eye Institute, University of Pennsylvania, Philadelphia, PA, USA*

[3]*Department of Clinical and Molecular Ophthalmogenetics, Netherlands Institute for Neuroscience, an institute of the Royal Netherlands Academy of Arts and Sciences, Amsterdam, The Netherlands*

[4]*Institute for Neurosciences of Montpellier, Hôpital Saint Eloi, Montpellier, France*

[5]*Division of Clinical Genetics, Innsbruck Medical University, Innsbruck, Austria*

[§]*Present address: Department of Physiology, Dartmouth Medical School, Hanover, NH, USA*

* authors contributed equally to this work

Correspondence to: Katja Koeppen

Dartmouth Medical School

Department of Physiology

604 Remsen Building

Hanover, NH 03755

USA

Phone: (603) 650-1534

Fax: (603) 650-1130

E-mail: Katja.UU.Koeppen@Dartmouth.edu

For Peer Review

Abstract

The *CNGA3* gene encodes the A3 subunit of the cone photoreceptor cyclic nucleotide-gated (CNG) channel, an essential component of the phototransduction cascade. Certain mutations in *CNGA3* cause autosomal recessive achromatopsia, a retinal disorder characterized by severely reduced visual acuity, lack of color discrimination, photophobia and nystagmus. We identified three novel mutations in the pore-forming region of CNGA3 (L363P, G367V and E376K) in patients diagnosed with achromatopsia. We assessed the expression and function of channels with these three new and two previously described mutations (S341P and P372S) in a heterologous HEK293 cell expression system using Western blot, subcellular localization on the basis of immunocytochemistry, calcium imaging and patch clamp recordings. In this first comparative functional analysis of disease-associated mutations in the pore of a CNG channel, we found impaired surface expression of S341P, L363P and P372S mutants and reduced macroscopic currents for channels with the mutations S341P, G367V and E376K. Calcium imaging and patch clamp experiments after incubation at 37°C revealed non-functional homo- and heteromeric channels in all five mutants, but incubation at 27°C combined with co-expression of the B3 subunit restored residual function of channels with the mutations S341P, G367V and E376K.

Key words: achromatopsia, CNG channel, CNGA3, pore mutation

For Peer Review

Introduction

Cyclic nucleotide-gated (CNG) channels are ligand-activated, non-selective cation channels that belong to the superfamily of voltage dependent K^+ channels. In contrast to other members of this superfamily, CNG channels are barely voltage-dependent, but mainly activated through ligand binding. CNG channels are key components of neurosensory signal transduction in the olfactory epithelium as well as in retinal rod and cone photoreceptors. Native cone CNG channels are tetramers of two A3 and two B3 subunits (Matveev, et al., 2008; Peng, et al., 2004), which are structurally homologous proteins composed of six transmembrane helices (S1-S6), a pore-forming region between S5 and S6, a cyclic nucleotide-binding domain (CNBD) and a C-linker region between S6 and the CNBD, which mediates channel gating (Fig. 1).

In contrast to the B3 subunit, the A3 subunit forms functional homomeric channels when expressed in heterologous systems. However, the modulatory B3 subunit has an essential role *in vivo*. It has been shown for rod photoreceptors that CNGB1 is required for targeting of CNGA1 to rod outer segments (Huttl, et al., 2005; Kizhatil, et al., 2009) and CNGB3 could have a similar function in cones.

Mutations in the genes encoding the subunits of the cone photoreceptor CNG channel, *CNGA3* (OMIM #600053) and *CNGB3* (OMIM #605080), are associated with autosomal recessive achromatopsia (ACHM2, OMIM #216900). Achromatopsia is a rare congenital retinal disorder characterized by lack of color discrimination, severely reduced visual acuity, photophobia and nystagmus. Most patients present with complete achromatopsia (rod monochromatism, total color blindness), but sometimes the phenotype is described as incomplete achromatopsia with milder symptoms and residual cone function.

Here we report the identification of three new point mutations in the pore region of CNGA3: L363P, G367V and E376K, and we present the results of a detailed functional

For Peer Review

characterization of these three new as well as two previously described mutations (S341P and P372S) located in the pore region of the cone CNG channel.

The investigation of naturally occurring pore mutations (e.g. those found in achromatopsia patients) helps to define the concrete function of individual amino acid residues thus enhancing our understanding of the molecular properties of the pore and elucidating mutation-associated pathomechanisms.

We pursued our objective by comparatively analyzing the effects of single amino acid substitutions in the pore region of CNGA3 on channel function. For that purpose, mutant channels were heterologously expressed in HEK293 cells and their functional properties and surface expression were analyzed using calcium imaging, patch clamp recordings and immunocytochemistry.

Subjects, Materials and Methods

Patients and genetic analysis

Patients diagnosed with achromatopsia were referred by different ophthalmic or medical genetic centers and registered at the Molecular Genetics Laboratory, Institute for Ophthalmic Research, Tuebingen, Germany. The clinical diagnoses were based on ophthalmic examinations including ERG recordings, visual acuity measurements and standard color vision testing. The study conformed to the tenets of the Declaration of Helsinki and received approval from the Ethical Committee of the University of Tuebingen. Patients and relatives were informed about the objectives of the study and venous blood samples were taken for genetic analysis upon informed consent. Total genomic DNA was extracted from the blood samples according to standard procedures.

Patients' DNA was screened for mutations in the coding exons and flanking intronic sequences of the CNGA3 gene as reported previously (Kohl, et al., 1998; Wissinger, et al., 2001). Gene variants and mutations were designated according to the guidelines of the Human

For Peer Review

Genome Variation Society (http://www.hgvs.org/mutnomen). Segregation analysis for the presence and independent inheritance of two mutant alleles was performed in all available patients' parents and siblings by direct sequencing of the relevant gene segment. All newly identified mutations were confirmed in two independent PCR amplifications by DNA sequencing. Additionally, 100 persons with normal vision were screened as controls for the presence of the identified mutations by sequencing of exon 7 of CNGA3 using the following primers: F703 (5'-GCATACTGTGTAGCCGTGAGG-3'), FEO239 (5'-TGGCAGCTACTTCGGGGA GA-3'), FEO248 (5'-GTGGGCAATGTGGGCTCC-3') and FEO91 (5'-CTCTTTGAATTC TTTGACCGCAC-3').

Expression of mutant A3 channels

Wild-type human *CNGA3* (RefSeq NM_001298.2) and *CNGB3* (RefSeq NM_019098.3) expression constructs were generated as described previously (Trankner, et al., 2004). Mutant human *CNGA3* expression constructs were obtained by *in vitro* mutagenesis applying the QuikChange Site-Directed Mutagenesis Kit (Stratagene, La Jolla, CA, USA) using the full-length wild-type *CNGA3* cDNA cloned into the pcDNA3.1/Zeo(+) vector as a template. Correct sequences of the cDNA inserts were confirmed by automated DNA sequencing on an ABI PRISM 3100 Genetic Analyzer (Applied Biosystems, Foster City, CA, USA). Column-purified expression constructs were used to transfect human embryonic kidney 293 (HEK293) cells employing Lipofectamine 2000 (Invitrogen, Carlsbad, CA, USA) according to the manufacturer's protocol. For calcium imaging and patch clamp measurements, the cells were co-transfected with the cyan fluorescent protein (CFP) expression vector pECFP-C1 (Clontech, Mountain View, CA, USA) to distinguish transfected from untransfected cells. For the expression of homomeric channels we used 8 µg CNGA3 construct and 2 µg CFP plasmid, whereas in co-expression experiments, 3 µg CNGA3 and 5 µg CNGB3 constructs were combined with 1.25 µg of the CFP plasmid. After transfection, cells were transferred to poly-L-lysine-coated coverslips and incubated at 37°C or 27°C in DMEM including 10 %

For Peer Review

Fetal Bovine Serum, 1 % Penicillin/Streptomycin and 1 % Fungizone (Gibco/Invitrogen, Carlsbad, CA, USA) at 5 % CO_2. Cells were treated with 3 mM sodium butyrate (Sigma-Aldrich, St. Louis, MO, USA) for 24-48 h starting one day post transfection. Measurements were conducted 2-3 days after transfection on CFP-positive cells.

Primary functional analysis – calcium imaging

Mutant human A3 channels were expressed either alone or together with wild-type B3 subunit and the function of the channels was analyzed by calcium imaging using a Zeiss Axioskop (Carl Zeiss AG, Jena, Germany) equipped with an imaging system from Visitron Systems (Puchheim, Germany) and the Metafluor 6.2 Imaging Software (Universal Imaging/Molecular Devices, Downingtown, PA, USA). Transfected HEK293 cells were loaded with the Ca^{2+}-sensitive fluorescent dye fura-2 (Grynkiewicz, et al., 1985) by incubation in extracellular solution (150 mM NaCl, 5 mM KCl, 2 mM $CaCl_2$, 2 mM $MgCl_2$, 10 mM HEPES and 30 mM Glucose) containing 4 µM fura-2-acetomethoxyester and 0.04 % Pluronic (Molecular Probes/Invitrogen, Carlsbad, CA, USA) for 20-30 min at 37°C or 27°C. Fluorescence was recorded prior to and after induction with the membrane permeable cGMP-analog 8-bromoguanosine-3' 5'-cyclic monophosphate (8-Br-cGMP; BIOLOG Life Science Institute, Bremen, Germany). The final 8-Br-cGMP concentration in the bath solution was 10 mM. For each mutation, 20-30 CFP fluorescent cells were analyzed in at least 2 separate measurements.

Western blot and immunocytochemistry

For Western blot experiments enriched membrane fractions were obtained by centrifugation of HEK293 cell lysates. Membrane fractions of transfected and non-transfected cells were separated on a NuPAGE 4-12 % Bis-Tris Gel (Invitrogen, Carlsbad, CA, USA) (15 µg protein per lane). Blots were blocked with 5 % milk powder solution, probed with the CNGA3 antibody SA3900 (1:1000) (Koeppen, et al., 2008) or anti-β-actin (1:4000; Chemicon/Millipore, Billerica, Ma, USA) as loading control and an anti-rabbit IgG

John Wiley & Sons, Inc.

For Peer Review

horseradish peroxidase-linked secondary antibody (1:4000; Amersham Biosciences, Arlington Heights, IL, USA) and anti-mouse IgG horseradish peroxidase-linked secondary antibody (1:10 000, Calbiochem/Merck, Darmstadt, Germany), respectively.

HEK293 cells were transfected as described above to analyze the integration of mutant channels into the plasma membrane. Treatment of transfected cells with 3 mM sodium butyrate (Sigma-Aldrich, St. Louis, MO, USA) was performed only with cells expressing $A3_{L363P}$ + B3. Immunocytochemical staining was performed 48h after transfection as described previously (Reuter, et al., 2008). The cell membrane of HEK293 cells was stained using an Alexa-488 coupled anti-wheat germ agglutinin (WGA) antibody (1:75; Molecular Probes/Invitrogen, Carlsbad, CA, USA). CNG channels were detected with an anti-CNGA3 primary antibody SA3900 (1:250) (Koeppen, et al., 2008) and an Alexa-660 labeled goat anti-rabbit antibody (1:250; Molecular Probes/Invitrogen, Carlsbad, CA, USA). Image acquisition was done using the Axio Imager Z1 System with Apotome (Carl Zeiss AG, Oberkochen, Germany). Z-stacks of labeled cells were recorded with distances of 0.2 – 0.3 µm at 63x magnification. The image data were analyzed with Axio Vision Rel. 4.8 (Carl Zeiss AG, Oberkochen, Germany) and ImageJ 1.43m (Rasband WS, ImageJ, National Institute of Health, Bethesda, MD, USA). To establish fluorescence profiles, the fluorescence intensities of the stained plasma membrane and the CNG channels were measured along a line tool using Axio Vision Rel. 4.8 (Carl Zeiss AG, Oberkochen, Germany) in one slice of the Z-stack. The fluorescent intensities were normalized to the maximum intensity of each channel and plotted against the distance of the line tool using Microsoft Office Excel 2007.

Tools of ImageJ 1.43m (Rasband WS, ImageJ, National Institute of Health, Bethesda, MD, USA) were used to assess the degree of co-localization of wild-type and mutant channels with the plasma membrane. The background of the WGA-Alexa 488 as well as the CNGA3-Alexa 660 staining was subtracted using the "BG subtraction from ROI" plugin. Subsequently, the cell membrane of a cell that expressed CNG channels was selected using the region of interest

For Peer Review

tool and the Manders'overlap coefficient was calculated with the "Manders coefficients" plugin. For wild-type and mutant channels at 27 °C and 37 °C at least 9 cells were analyzed. Data are presented as mean ± SD. For statistical evaluation the Mann-Whitney rank sum test was performed using MYSTAT 12 Version 12.02.00 (SYSTAT Inc., Chicago, IL, USA).

Functional analysis – patch clamp recordings

Mutant channels were further analyzed with the patch clamp technique (Hamill, et al., 1981) using glass pipettes with initial resistances of 3-5 MΩ to obtain excised inside-out patches. A series of 300 ms-voltage pulses was applied in 20 mV steps from -80 to +80 mV. For generating cGMP dose-response relationships, macroscopic currents were recorded under symmetric ionic conditions (100 mM KCl, 25 mM KOH, 10 mM EGTA and 10 mM HEPES, pH 7.4). Inside-out patches were superfused with various concentrations of cGMP (3 -1000 µM; Sigma-Aldrich, St. Louis, MO, USA). The solution applied to the intracellular side of the patch additionally contained 10 mM glucose. Current traces were recorded at room temperature with an Axon CNS Axopatch 200B amplifier with Digidata 1440A (Molecular Devices, Sunnyvale, CA, USA) and passed through a 10 kHz band-pass as well as a 2 kHz low-pass filter. For the ion selectivity assay, the pipette solution contained 105 mM NaCl, 2.5 mM NaOH, 1 mM EGTA and 10 mM HEPES, pH 7.4. Application solutions contained 105 mM of either NaCl, KCl, LiCl or CsCl, 2.5 mM NaOH, 1 mM EGTA, 10 mM HEPES and 10 mM glucose.

The Clampex 10.1 software was used for data acquisition (Molecular Devices, Sunnyvale, CA USA). Mean values for each of the nine current traces were obtained by averaging the values for each trace with Clampfit 10.1 (Molecular Devices). Leak currents recorded in the absence of ligand were subtracted from currents in the presence of ligand. With these data, dose-response relationships for the activation of mutant channels by cGMP were calculated utilizing the Sigma Plot Software (SPSS Inc., Chicago, IL, USA).

For Peer Review

The normalized curves were fitted as a function of the agonist concentration using the Hill equation to calculate the agonist concentration of half-maximum activation ($K_{1/2}$ value) and the Hill coefficient h. Ion selectivity recordings were used to generate I/V-curves for different monovalent ions at saturating cGMP concentrations. For this purpose, the mean current for each ion at a given voltage was calculated using Microsoft Excel and plotted against the corresponding membrane potential. In order to compare the permeability of the channel for different monovalent cations at positive and negative membrane potentials, currents were normalized to the Na^+ current. Data are presented as mean ± SD. Statistical significance was determined by the unpaired t-test for dose-response relationships or two-way ANOVA for ion selectivity measurements using GraphPad Prism 5.0c for Mac OS X (GraphPad Software, San Diego, CA, USA). A two-tailed p-value < 0.05 was considered statistically significant (*), $p = 0.001$-0.01 very significant (**) and $p < 0.001$ extremely significant (***).

Results

Identification of mutations in the pore of CNGA3 and patients' phenotypes

In our ongoing genetic screenings of the *CNGA3* gene in patients affected by autosomal recessively inherited achromatopsia, we were able to identify 14 patients from 11 independent families who were found to carry either a homozygous or a compound heterozygous mutation in the pore-forming region of *CNGA3*. Four patients in this group had been reported previously (Wissinger, et al., 2001), while ten patients were newly identified. Segregation analysis was performed in all cases except for patients CHRO367-2641, CHRO389-13406, CHRO532-16588 and CHRO544-16904, for whom no relatives were available for analysis. Table 1 lists the *CNGA3* genotypes and some relevant clinical data from the patients. For nearly half of the patients (6/14) a clinical diagnosis of complete achromatopsia has been established. These patients have photophobia, variable degrees of nystagmus, severely decreased visual acuity (0.04–0.10), and absent photopic ERG responses with normal scotopic

For Peer Review

responses. Patients who could perform psychophysical testing had no color vision; some patients were too young for formal testing. One patient (family CHRO119) showed residual cone function in photopic ERG recordings, abnormal color vision, a slightly better visual acuity (0.2) and only moderate photophobia and was diagnosed with incomplete achromatopsia (Wissinger, et al., 2001). Seven predominantly very young patients could not be clearly classified as to type of achromatopsia.

The majority of patients (10/14) were homozygous, while four were compound heterozygous for mutations in *CNGA3* (Table 1). We found the previously published mutations c.1021T>C / p.S341P and c.1114C>T / p.P372S in three of the new patients. In addition, three novel missense mutations c.1088T>C / p.L363P, c.1100G>T / p.G367V and c.1126G>A / p.E376K, were identified in seven of the patients (five index patients and two affected siblings, Supp. Table S1). All these patients were truly homozygous for the respective mutation as confirmed by segregation analyses within the families for those patients of whom parents were available for analysis. All mutations were excluded in 100 control subjects (200 chromosomes) by direct sequencing of exon 7 of *CNGA3*.

The mutations L363P and E376K were each detected in homozygous state in single families (CHRO301 and CHRO383). Four patients from three families (CHRO293, CHRO356 and CHRO389) were found to be homozygous for the mutation G367V. The previously reported mutation S341P was found in one additional patient in combination with the mutation R277G on the second allele, while the mutation P372S was found in two additional patients in homozygous and in one patient in compound heterozygous state together with the mutation R283W on the other allele.

The mutations L363P, G367V and P372S affect amino acid positions that are evolutionary fully conserved in human, bovine, murine and chicken CNGA3, human and bovine CNGA1, as well as human KCNH2 (HERG channel). Moreover, G367 and P372 are also conserved in

For Peer Review

the bacterial KcsA channel. The amino acid positions S341 and E376 are highly conserved among the CNGA3 subunits of the different species (Fig. 1).

The serine residue at position 341 is situated in the pore turret. Positions L363 and P372 are located just before and just after the selectivity filter, respectively, while amino acid G367 is in the middle of the selectivity filter signature sequence. Amino acid residue E376 is located in the transitional region between pore and S6 transmembrane domain (Fig. 2).

To investigate the effect of these five mutations in the pore region of CNGA3 on channel function, we expressed mutant channels in HEK293 cells and performed calcium imaging, patch clamp recordings and immunocytochemical experiments.

Functional analysis – calcium imaging

Calcium imaging experiments using the Ca^{2+}-sensitive fluorescent dye fura-2 and 10 mM 8-Br-cGMP were performed to determine whether the mutant channels possessed residual calcium permeability. Neither of the five mutant channels mediated any 8-Br-cGMP-induced calcium influx when expressed alone or together with the wild-type B3 subunit after incubation of transfected cells at 37°C (Table 2). After lowering the incubation temperature of transfected cells to 27°C, calcium influxes could be observed for heteromeric (but not homomeric) channels with the A3 mutations S341P, G367V and E376K. However, compared with the wild-type channel, a much smaller fraction of transfected cells responded. The inclusion criterion for a positive response was an increase in the fluorescence ratio (380 nm/340 nm) by at least 0.1. The partial rescue of mutant channel function after incubation of transfected cells at 27°C is thought to originate from the restoration of protein folding and surface expression at lower temperatures (Denning, et al., 1992; Paulussen, et al., 2002; Rajamani, et al., 2002; Reuter, et al., 2008; Zhou, et al., 1999).

In contrast, channels with the mutations L363P or P372S did not show any responses in calcium imaging measurements.

Western blot and immunocytochemistry

For Peer Review

Western blot experiments confirmed that all five channel mutants were expressed in HEK293 cells (Supp. Figure S1). Protein levels for $A3_{S341P}$ and $A3_{L363P}$ were somewhat lower, possibly as a result of reduced protein stability. Co-localization experiments were performed to assess whether changing the incubation temperature of transfected HEK293 cells could affect the integration of mutant channels into the plasma membrane (Fig. 3, Supp. Figures S2 and S3 and Supp. Table S2).

To quantify the extent of co-localization of mutant channels with the cell membrane we calculated the Manders' overlap coefficient (Zinchuk and Grossenbacher-Zinchuk, 2009). Usually, coefficients in the range of 0.6 – 1.0 are considered to indicate co-localization. This range was hardly reached with the wild-type channels. Thus, taking the results from our functional analyses into account, Manders' overlap coefficients of 0.5 were also considered to indicate co-localization under our experimental conditions.

As expected, homomeric wild-type channels co-localized with the cell membrane at both temperatures. In comparison with the wild-type all homomeric mutants showed reduced membrane co-localization coefficients. Lowering the cultivation temperature had no effect on the five analyzed homomeric mutant channels. In the next step, the effect of the wild-type B3 subunit on plasma membrane targeting of mutant heteromeric channels was analyzed. The presence of the B3 subunit improved the membrane targeting in the case of $A3_{E376K}$ + B3 at both temperatures and for $A3_{G367V}$ + B3 and $A3_{P372S}$ + B3 at 27°C but not at 37°C (Supp. Table S2 and Supp. Figure S3). The membrane localization of the mutant $A3_{S341P}$ was unaffected by the B3 subunit. Surprisingly, the co-localization with the plasma membrane of $A3_{L363P}$ was impaired by the presence of the B3 subunit at 37°C. Altogether, homomeric as well as heteromeric mutant channels showed significantly lower incorporation into the plasma membrane compared to wild-type channels with the exceptions of $A3_{G367V}$ + B3 at 27°C and $A3_{E376K}$ + B3 at 27°C and 37°C.

For Peer Review

Functional analysis – patch clamp recordings

Calcium imaging measurements only provide information about the calcium permeability of mutant channels. For a more detailed functional characterization of channel mutants that showed residual channel function due to calcium permeability, we performed patch clamp recordings to evaluate the electrophysiological properties of the mutant channels with regard to the apparent agonist affinity and permeability for various monovalent cations.

For patch clamp experiments, mutant channels were expressed as heteromers ($A3_{mut}$ + B3) and transfected cells were cultivated at 27°C. Control measurements with $A3_{wt}$ + B3 channels after incubation at 37°C or 27°C showed that the lower incubation temperature did not change the electrophysiological properties of wild-type channels (parameters for 37°C: $K_{1/2}$ = 18.50 ± 1.60, h = 1.29 ± 0.18; N = 6 and 27°C: $K_{1/2}$ = 17.96 ± 1.71, h = 1.17 ± 0.12; N = 7).

a) cGMP dose-response relationships

Dose-response relationships for activation of channels by cGMP were generated for the three mutants that showed residual function in calcium imaging experiments: $A3_{S341P}$ + B3, $A3_{G367V}$ + B3 and $A3_{E376K}$ + B3 (Fig. 4). The agonist concentration for half-maximum activation ($K_{1/2}$ value) and the Hill coefficient h were calculated by fitting of the dose-response curves with the Hill equation (Table 3). Statistical analysis using an unpaired t-test showed that the $K_{1/2}$ values of $A3_{S341P}$ + B3 and $A3_{E376K}$ + B3 were not significantly different from that of the wild-type channel while the 2.5-fold shift of the dose-response curve towards higher cGMP concentrations for $A3_{G367V}$ + B3 proved to be statistically significant (p = 0.006). For $A3_{E376K}$ + B3 the slope of the dose-response curve was steeper compared with those of the wild-type and the other two mutants, indicating an altered cooperativity in ligand binding.

Notably, all three channel mutants yielded strongly reduced macroscopic currents compared with heteromeric wild-type channels (compare Fig. 5A & Supp. Figure S4).

No cGMP-induced potassium currents could be observed for $A3_{L363P}$ + B3 and $A3_{P372S}$ + B3 (N = 20 inside-out patches per mutation).

For Peer Review

b) Selectivity for monovalent cations

To assess whether the analyzed mutations in the pore region of CNGA3 alter the selectivity of the channel for monovalent cations, K^+, Na^+, Li^+ and Cs^+ currents were measured in the presence of 1000 µM cGMP for $A3_{G367V}$ + B3, $A3_{E376K}$ + B3 and $A3_{wt}$ + B3. For $A3_{S341P}$ + B3, the ion selectivity could not be determined, since the macroscopic currents obtained from patches expressing these channels were too small.

For $A3_{G367V}$ + B3 a pronounced outward rectification was observed in the presence of all four analyzed monovalent ions (Fig. 5A + C) compared to $A3_{wt}$ + B3 (Fig. 5A + B). Permeability ratios for wild-type and mutant channels are listed in Table 4. The ion selectivity of $A3_{E376K}$ + B3 was identical to that of the wild-type channel with a selectivity sequence of $K^+ > Na^+ >> Li^+ > Cs^+$ at positive and negative membrane potentials (Fig. 5D + E). In contrast, at +80 mV $A3_{G367V}$ + B3 featured a statistically significant increase in permeability for K^+ and Cs^+ (Fig. 5C), resulting in an altered selectivity sequence: $K^+ >> Na^+ > Cs^+ > Li^+$.

c) Electrophysiology of homomeric channels with the mutations G367V and E376K

For $A3_{G367V}$ and $A3_{E376K}$ patch clamp recordings were performed on cells expressing homomeric channels to assess whether these mutants possess a residual conductivity for potassium ions in the homomeric state. However, no cGMP-evoked potassium currents could be detected for either of the two channel mutants in recordings from 20 inside-out patches per mutation.

Discussion

In this study we present a first comparative functional characterization of disease-associated mutations in the pore of a cyclic-nucleotide gated channel. This included three new CNGA3 mutations identified in this study (L363P, G367V and E376K) as well as two previously described mutations (S341P and P372S), all associated with autosomal recessively inherited achromatopsia. So far, only one disease causing mutation in the pore region of CNGA3 had

For Peer Review

been functionally analyzed: T369S (Trankner, et al., 2004). This mutation was found in two sisters with a mild form of incomplete achromatopsia and considerably preserved cone function. Patch clamp analysis revealed that $A3_{T369S}$ + B3 channel function is mainly intact, with only subtle changes in ion permeability.

The results of our functional characterizations confirm that the five newly analyzed mutations are in fact pathogenic and are unlikely to mediate residual cone function under physiological conditions. With the exception of patients from families CHRO119, CHRO301 and CHRO544, who had a slightly better visual acuity and possibly residual cone function in the ERG and some remaining color discrimination ability, the clinical symptoms are in line with a diagnosis of complete achromatopsia. The residual cone function of patient CHRO119 may result from the second mutant allele (R223W) in this compound heterozygous patient. The clinical evidence for a low level of residual cone function in the two young siblings from CHRO301, who are homozygous for the L363P mutation, could not be supported by our functional data and may result from some photoreceptor specific compensatory mechanisms.

A mutation in the pore region of CNGA3 could lead to one or more of the following potential consequences: a) misfolding of the protein leading to reduced surface expression and/or impaired function, b) altered size or charge of the ion permeation pathway, c) disruption of intrasubunit interactions required for gating, and d) disturbed rotational movement of the pore helix during gating.

The CNG channel pore is formed by a loop between transmembrane domains S5 and S6, which features a re-entrant pore helix followed by a putative selectivity filter. Within the selectivity filter, K^+ channels posses a highly conserved signature sequence (TXXTXGYG, Fig. 1), which is partially also conserved within CNGA3 and CNGA1 subunits (Heginbotham, et al., 1992). Deleting the latter two amino acids of this motif (-YG-) in *Shaker* K^+ channels renders the mutant K^+ channel non-selective for cations and blockable by divalent cations (Heginbotham, et al., 1992) thus reflecting the native sequence motif of CNG

For Peer Review

channels as well as their permeability for various monovalent and divalent cations (Liu and Siegelbaum, 2000). While the pore helix itself does not line the permeation pathway (Doyle, et al., 1998), it has been shown to undergo large conformational changes associated with gating (Liu and Siegelbaum, 2000). During channel opening, the pore helix rotates around its long axis, so that this region is involved in both ion permeation and gating.

A recent cysteine substitution scan of residues in the pore helix suggests that in contrast to voltage-activated potassium channels, the activation gate of CNG channels is not located at the intracellular end of the last transmembrane segment. Instead, the selectivity filter itself appears to act as the primary gate in CNG channels, with the highest energetic barrier for ion permeation being somewhere in the middle of the filter (Contreras, et al., 2008).

In a previous publication, homomeric A3 channels with the mutation **S341P** or **P372S** were described to be non-functional after incubation at 37°C (Muraki-Oda, et al., 2007). In contrast to these earlier results, we performed co-expression experiments of mutant A3 and wild-type B3 subunits and incubated transfected cells at a lower temperature of 27°C. Under these conditions, we were able to detect a residual function of $A3_{S341P}$ + B3 channels in calcium imaging and patch clamp experiments, whereas $A3_{P372S}$ + B3 mutants were still non-functional. Substitutions in bovine CNGA1 in a position corresponding to P372 in human CNGA3 leads to a loss of channel function when proline is replaced by cysteine or valine (Gamel and Torre, 2000). In contrast to that, the substitution by alanine results in the formation of channels, which are strongly voltage-gated (Martinez-Francois, et al., 2009). The proline is also conserved within K^+ channels and HERG channels (Fig. 1) and in the latter case the substitution by cysteine strongly affects normal channel function (Liu, et al., 2002; Tseng, et al., 2007). The Manders'overlap coefficient calculated for WGA membrane staining versus anti-CNGA3 immunostaining as a parameter for membrane localization was similar for $A3_{P372S}$ + B3 and $A3_{S341P}$ + B3 channels at 27°C (Supp. Table S2), the latter still being functional under those conditions. Thus, the non-functionality of the P372S mutant seems to

For Peer Review

be a result of the combination of diminished membrane targeting and impaired protein function. The assumption that the severely diminished currents of $A3_{S341P}$ + B3 are a result of impaired surface expression of $A3_{S341P}$ could be confirmed in immunocytochemical co-localization experiments. The replacement of serine 341 by proline leads to the loss of a glycosylation site, which might explain the reduced targeting of mutant channels to the plasma membrane as well as the reduced overall protein expression/stability. This could also explain the incapability of the B3 subunit to improve membrane targeting of heteromeric channels while still improving channel function at least at 27°C (Supp. Table S2 and Table 2).

The amino acid position **G367** is part of the K^+ channel signature sequence in the selectivity filter and is highly conserved across different ion channel types and species. This glycine residue is an important structural determinant that may force a turn in the pore loop (Becchetti, et al., 1999) and appears to be implicated in the rotational movement of the pore helix, a conformational change mediating the alteration between conductive and non-conductive states of the channel (Contreras, et al., 2008). Thus, a cysteine substitution at the corresponding position in bCNGA1 (G362) did not yield functional channels (Contreras, et al., 2008). G367 is directly adjacent to E368, which forms the binding site for external divalent cations and thereby mediates the block of CNG channels by Ca^{2+} and Mg^{2+} (Eismann, et al., 1994; Root and MacKinnon, 1993). While it would have been intriguing to assess the calcium block of channels with the mutation G367V, this analysis could not be performed due to the extremely low macroscopic currents obtained from patches containing these channels (Fig. 5A and Supp. Figure S4).

The pore diameter of CNG channels is about 5 Å in the open state (Giorgetti, et al., 2005) and thus much wider than the pore of sodium or potassium channels, but comparable to the pore size of other non-selective cation channels like the acetylcholine receptor channel (Hille, 1992). Since G367 is located at the narrowest point of the channel pore (Fig. 2), the substitution of a glycine by a larger valine residue can be assumed to affect the pore size and

For Peer Review

thus the permeation pathway. This could explain the pronounced outward rectification and severely reduced macroscopic currents as well as the increased current noise observed for $A3_{G367V}$ + B3. A recent study using bCNGA1 suggests that hydrophobic intrasubunit interactions between the amino acid residues homologous to the hCNGA3 residues L361 and F385 enable the coupling of the pore wall to the pore helix. The interaction of T360 and E368 (Fig. 2) is essential for the coupling of the pore helix to the S6 transmembrane domain. Thus, the movement of S6 upon ligand binding is transferred to the pore during gating. (Mazzolini, et al., 2009). A mutation in position 367 could impair the interaction between amino acid residues T360 and E368 and interfere with channel gating. This would also explain the reduced cGMP sensitivity that was observed for $A3_{G367V}$.

The amino acid position **E376** is situated in the transitional region between pore and S6 transmembrane domain. During gating the movement of the C-Linker is transmitted to the S6 transmembrane domain resulting in a rotation of the upper part of the S6 transmembrane domain (Giorgetti, et al., 2005). Therefore, the exchange of a negatively charged glutamate by a positively charged lysine at this position could result in improper folding. This can be supported by the fact that channel function of $A3_{E376K}$ can be partially restored under conditions that promote proper folding (e.g. co-expression of the B3 subunit and reduced incubation temperature of transfected cells).

So far, no crystal structure has been obtained for CNGA3 or other CNG channels, which impedes the prediction of the effects of mutations in the pore region on channel structure and function. However, there is a certain degree of structural homology to related ion channels that have been studied using X-ray crystallography. For instance, there is evidence that the structure of the C-terminal end of the CNG channel pore region (E368-P371) is similar to that of KcsA (Doyle, et al., 1998). In contrast, some other regions seem to deviate from the structure observed for KcsA: one example is the external accessibility of the residue corresponding to **L363** in bovine CNGA1 (bCNGA1) (Liu and Siegelbaum, 2000), while the

For Peer Review

homologous residue in KcsA was found to be located at the inner end of the pore helix, near the central cavity of the pore (Doyle, et al., 1998). Mutating the residue corresponding to L363 in bCNGA1 to cysteine or alanine does not yield functional homomeric channels (Becchetti and Gamel, 1999; Martinez-Francois, et al., 2009). However, a cysteine substitution study by (Liu and Siegelbaum, 2000) showed that channel function could be rescued when expressing the cysteine mutant as a tandem dimer with the wild-type channel. In contrast, our experiments showed that the presence of wild-type B3 (which is closer to the native situation) is not sufficient to allow for any residual channel function with the A3 mutation L363P. Additionally, homomeric as well as heteromeric channels with this mutation exhibited significantly disturbed surface expression (Supp. Table S2). A possible explanation for the loss of function is that a mutation in position 363 could disrupt the interaction of E368 and T360, which anchors the pore wall to the pore helix (Mazzolini, et al., 2009). This intrasubunit interaction is assumed to be responsible for keeping the pore in shape and is probably required for gating. Therefore, it is likely that the mutation L363P renders the channel non-functional, especially since a proline substitution is likely to disturb the structure of the pore helix.

In conclusion, our functional analyses reveal that different mutations in the pore region of CNGA3 lead to diverse functional defects. $A3_{L363P}$ and $A3_{P372S}$ showed complete absence of channel function due to impaired surface expression in combination with disturbed protein folding especially in the latter case. Reduced integration of mutant channels into the plasma membrane was also observed for $A3_{S341P}$ alongside with severely diminished maximum currents of $A3_{S341P}$ + B3 channels. The latter feature was also present in $A3_{E376K}$ + B3 and $A3_{G367V}$ + B3. In addition, $A3_{G367V}$ + B3 exhibited reduced cGMP sensitivity and altered ion selectivity. None of the five analyzed mutations mediated residual channel function under physiological conditions in a HEK293 cell expression system. However, a combination of reduced incubation temperature and co-expression with the B3 subunit restored residual

For Peer Review

function of channels with the mutations S341P, G367V and E376K, suggesting that the mechanism of disease in these cases involves aberrant protein folding. If this assumption is true, protein folding correctors might restore channel function *in vivo*.

Acknowledgements

The authors would like to thank all patients and family members for participating in this study. We also thank Thomas H. Hampton for comments on the manuscript and suggestions for the statistical analysis. This work was supported by a grant of the Deutsche Forschungsgemeinschaft [Wi1189/6-3 to B.W.].

References

Becchetti A, Gamel K. 1999. The properties of cysteine mutants in the pore region of cyclic-nucleotide-gated channels. Pflugers Arch 438(5):587-96.

Becchetti A, Gamel K, Torre V. 1999. Cyclic nucleotide-gated channels. Pore topology studied through the accessibility of reporter cysteines. J Gen Physiol 114(3):377-92.

Contreras JE, Srikumar D, Holmgren M. 2008. Gating at the selectivity filter in cyclic nucleotide-gated channels. Proc Natl Acad Sci U S A 105(9):3310-4.

Denning GM, Anderson MP, Amara JF, Marshall J, Smith AE, Welsh MJ. 1992. Processing of mutant cystic fibrosis transmembrane conductance regulator is temperature-sensitive. Nature 358(6389):761-4.

Doyle DA, Morais Cabral J, Pfuetzner RA, Kuo A, Gulbis JM, Cohen SL, Chait BT, MacKinnon R. 1998. The structure of the potassium channel: molecular basis of K+ conduction and selectivity. Science 280(5360):69-77.

Eismann E, Muller F, Heinemann SH, Kaupp UB. 1994. A single negative charge within the pore region of a cGMP-gated channel controls rectification, Ca2+ blockage, and ionic selectivity. Proc Natl Acad Sci U S A 91(3):1109-13.

John Wiley & Sons, Inc.

For Peer Review

Gamel K, Torre V. 2000. The interaction of Na(+) and K(+) in the pore of cyclic nucleotide-gated channels. Biophys J 79(5):2475-93.

Giorgetti A, Nair AV, Codega P, Torre V, Carloni P. 2005. Structural basis of gating of CNG channels. FEBS Lett 579(9):1968-72.

Grynkiewicz G, Poenie M, Tsien RY. 1985. A new generation of Ca2+ indicators with greatly improved fluorescence properties. J Biol Chem 260(6):3440-50.

Hamill OP, Marty A, Neher E, Sakmann B, Sigworth FJ. 1981. Improved patch-clamp techniques for high-resolution current recording from cells and cell-free membrane patches. Pflugers Arch 391(2):85-100.

Heginbotham L, Abramson T, MacKinnon R. 1992. A functional connection between the pores of distantly related ion channels as revealed by mutant K+ channels. Science 258(5085):1152-5.

Hille B. 1992. Ionic channels of excitable membranes. Sunderland, Mass.: Sinauer Associates.

Huttl S, Michalakis S, Seeliger M, Luo DG, Acar N, Geiger H, Hudl K, Mader R, Haverkamp S, Moser M and others. 2005. Impaired channel targeting and retinal degeneration in mice lacking the cyclic nucleotide-gated channel subunit CNGB1. J Neurosci 25(1):130-8.

Kizhatil K, Baker SA, Arshavsky VY, Bennett V. 2009. Ankyrin-G promotes cyclic nucleotide-gated channel transport to rod photoreceptor sensory cilia. Science 323(5921):1614-7.

Koeppen K, Reuter P, Kohl S, Baumann B, Ladewig T, Wissinger B. 2008. Functional analysis of human CNGA3 mutations associated with colour blindness suggests impaired surface expression of channel mutants A3(R427C) and A3(R563C). Eur J Neurosci 27(9):2391-401.

Kohl S, Marx T, Giddings I, Jagle H, Jacobson SG, Apfelstedt-Sylla E, Zrenner E, Sharpe LT, Wissinger B. 1998. Total colourblindness is caused by mutations in the gene encoding

For Peer Review

the alpha-subunit of the cone photoreceptor cGMP-gated cation channel. Nat Genet 19(3):257-9.

Liu J, Siegelbaum SA. 2000. Change of pore helix conformational state upon opening of cyclic nucleotide-gated channels. Neuron 28(3):899-909.

Liu J, Zhang M, Jiang M, Tseng GN. 2002. Structural and functional role of the extracellular s5-p linker in the HERG potassium channel. J Gen Physiol 120(5):723-37.

Martinez-Francois JR, Xu Y, Lu Z. 2009. Mutations reveal voltage gating of CNGA1 channels in saturating cGMP. J Gen Physiol 134(2):151-64.

Matveev AV, Quiambao AB, Browning Fitzgerald J, Ding XQ. 2008. Native cone photoreceptor cyclic nucleotide-gated channel is a heterotetrameric complex comprising both CNGA3 and CNGB3: a study using the cone-dominant retina of Nrl-/- mice. J Neurochem 106(5):2042-55.

Mazzolini M, Anselmi C, Torre V. 2009. The analysis of desensitizing CNGA1 channels reveals molecular interactions essential for normal gating. J Gen Physiol 133(4):375-86.

Muraki-Oda S, Toyoda F, Okada A, Tanabe S, Yamade S, Ueyama H, Matsuura H, Ohji M. 2007. Functional analysis of rod monochromacy-associated missense mutations in the CNGA3 subunit of the cone photoreceptor cGMP-gated channel. Biochem Biophys Res Commun 362(1):88-93.

Paulussen A, Raes A, Matthijs G, Snyders DJ, Cohen N, Aerssens J. 2002. A novel mutation (T65P) in the PAS domain of the human potassium channel HERG results in the long QT syndrome by trafficking deficiency. J Biol Chem 277(50):48610-6.

Peng C, Rich ED, Varnum MD. 2004. Subunit configuration of heteromeric cone cyclic nucleotide-gated channels. Neuron 42(3):401-10.

For Peer Review

Rajamani S, Anderson CL, Anson BD, January CT. 2002. Pharmacological rescue of human K(+) channel long-QT2 mutations: human ether-a-go-go-related gene rescue without block. Circulation 105(24):2830-5.

Reuter P, Koeppen K, Ladewig T, Kohl S, Baumann B, Wissinger B. 2008. Mutations in CNGA3 impair trafficking or function of cone cyclic nucleotide-gated channels, resulting in achromatopsia. Hum Mutat 29(10):1228-36.

Root MJ, MacKinnon R. 1993. Identification of an external divalent cation-binding site in the pore of a cGMP-activated channel. Neuron 11(3):459-66.

Trankner D, Jagle H, Kohl S, Apfelstedt-Sylla E, Sharpe LT, Kaupp UB, Zrenner E, Seifert R, Wissinger B. 2004. Molecular basis of an inherited form of incomplete achromatopsia. J Neurosci 24(1):138-47.

Tseng GN, Sonawane KD, Korolkova YV, Zhang M, Liu J, Grishin EV, Guy HR. 2007. Probing the outer mouth structure of the HERG channel with peptide toxin footprinting and molecular modeling. Biophys J 92(10):3524-40.

Wissinger B, Gamer D, Jagle H, Giorda R, Marx T, Mayer S, Tippmann S, Broghammer M, Jurklies B, Rosenberg T and others. 2001. CNGA3 mutations in hereditary cone photoreceptor disorders. Am J Hum Genet 69(4):722-37.

Zhou Z, Gong Q, January CT. 1999. Correction of defective protein trafficking of a mutant HERG potassium channel in human long QT syndrome. Pharmacological and temperature effects. J Biol Chem 274(44):31123-6.

Zinchuk V, Grossenbacher-Zinchuk O. 2009. Recent advances in quantitative colocalization analysis: focus on neuroscience. Prog Histochem Cytochem 44(3):125-72.

For Peer Review

Figure Legends

Figure 1. Structure of the CNGA3 subunit and sequence alignment of the pore region

The topological model of the CNGA3 polypeptide depicts six transmembrane helices (S1-S6), a pore region and a C-linker connecting pore region and cyclic nucleotide-binding site (CNBD). The analyzed mutations in the pore region of the channel are depicted at their respective positions within the polypeptide. New mutations identified in this study are L363P, G367V and E376K. The alignment of the pore region shows the high evolutionary conservation of the mutated amino acid residues. GenBank accession numbers: Homo sapiens CNGA3 NP_001298.1, Bos taurus CNGA3 NP_776704.1, Mus musculus CNGA3 NP_034048.1, Gallus gallus CNGA3 NP_990552.1, Homo sapiens CNGA1 NP_000078.2, Bos taurus CNGA1 NP_776703.1, Homo sapiens KCNH2 NP_742053.1 and Streptomyces coelicolor KcsA NP_631700.1.

Figure 2. Schematic drawing of the pore-forming region of CNGA3. Depicted are two adjacent subunits and the locations of four of the analyzed mutations (black circles) as well as the positions of amino acid residues forming intrasubunit interactions (grey circles) within the pore region (Mazzolini, et al., 2009). Adapted from (Giorgetti, et al., 2005).

Figure 3. Analysis of the surface expression of wild-type and mutant A3 channels.

HEK293 cells were transfected with wild-type or mutant A3 plus wild-type B3 and incubated at either 37°C (top row) or 27°C (bottom row) for >24 h. The left column shows A3 channels stained with an Alexa Fluor 660-coupled secondary antibody (orange). The cell membrane labeling with WGA-Alexa Fluor 488 is depicted in the center column (green). Overlays of the two stainings are shown in the right micrograph column. Yellow lines in the overlay pictures indicate the axis along which the fluorescence intensities of the two fluorophors were

For Peer Review

determined. Fluorescence intensities were measured through a slice at the center of the cells at a distance of 0.2-0.3 µm and normalized to the maximum fluorescence intensity. The normalized fluorescence intensities (y-axis) of WGA-Alexa Fluor 488 (green line) and Alexa Fluor 660 (orange line) are plotted against the distance (x-axis) in the adjacent diagrams. Like $A3_{wt}$ + B3, $A3_{E376K}$ + B3 co-localized with the plasma membrane after incubation of transfected HEK293 cells at either temperature. Surface expression of $A3_{G367V}$ + B3 was impaired at 37°C, but not significantly different from wild-type channels at 27°C. For $A3_{L363P}$ + B3 and $A3_{P372S}$ + B3, membrane co-localization was impaired at both temperatures, but incubation of transfected cells at lower temperature led to an improvement of surface expression. In contrast to that, reduced surface expression of $A3_{S341P}$ + B3 could not be enhanced by lowering the cultivation temperature. The results of the quantification and statistical analysis of this data are displayed in Supp. Table S2.

Figure 4. cGMP dose-response relationships of heteromeric channels.

Macroscopic potassium currents were recorded from inside-out patches of transfected HEK293 cells under symmetric ionic conditions. Currents evoked by different concentrations of cGMP at a membrane potential of +80 mV were normalized to the maximum current (with 1000 µM cGMP) after subtraction of leak currents. Normalized currents are plotted against log [cGMP] as arithmetic means ± SD. Statistical analysis using an unpaired t-test showed that the dose-response relationship of $A3_{G367V}$ + B3 is significantly different from that of wild-type channels ($p = 0.006$) while the other two mutants did not deviate significantly. The following $K_{1/2}$ values have been calculated using the Hill equation: $A3_{S341P}$ + B3 (dashed line) = 26 µM, $A3_{G367V}$ + B3 (grey line) = 45 µM, $A3_{E376K}$ + B3 (dotted line) = 24 µM and $A3_{wt}$ + B3 (black line) = 18 µM.

For Peer Review

Figure 5. Selectivity for monovalent ions of pore mutants $A3_{E376K}$ + B3 and $A3_{G367V}$ + B3.

(A) Representative traces of cGMP-evoked currents through wild-type or mutant channels for various monovalent ions. Current traces were recorded over a time of 300 ms at membrane potentials from +80 mV to -80 mV in 20 mV increments at a saturating cGMP concentration. (B + C) Representative I/V plots of wild-type and mutant heteromeric channels. Macroscopic currents for monovalent ions are plotted against the membrane potential. Ion selectivity of $A3_{E376K}$ + B3 was similar to the wild-type (B). $A3_{G367V}$ + B3 showed an outward rectification and markedly reduced macroscopic currents (C). The selectivity sequences for outward and inward currents are $I_K > I_{Na} >> I_{Li} > I_{Cs}$ for $A3_{wt}$ + B3 and $A3_{E376K}$ + B3, but $I_K > I_{Na} > I_{Cs} > I_{Li}$ for $A3_{G367V}$ + B3.

Panels (D + E) show fractional currents of K^+, Li^+ and Cs^+ normalized to the Na^+ current at a membrane potential of +80 mV (D) and -80 mV (E). *** indicates statistically significant difference of $A3_{G367V}$ + B3 K^+ and Cs^+ permeability compared to wt as determined with two-way ANOVA ($p < 0.001$).

For Peer Review

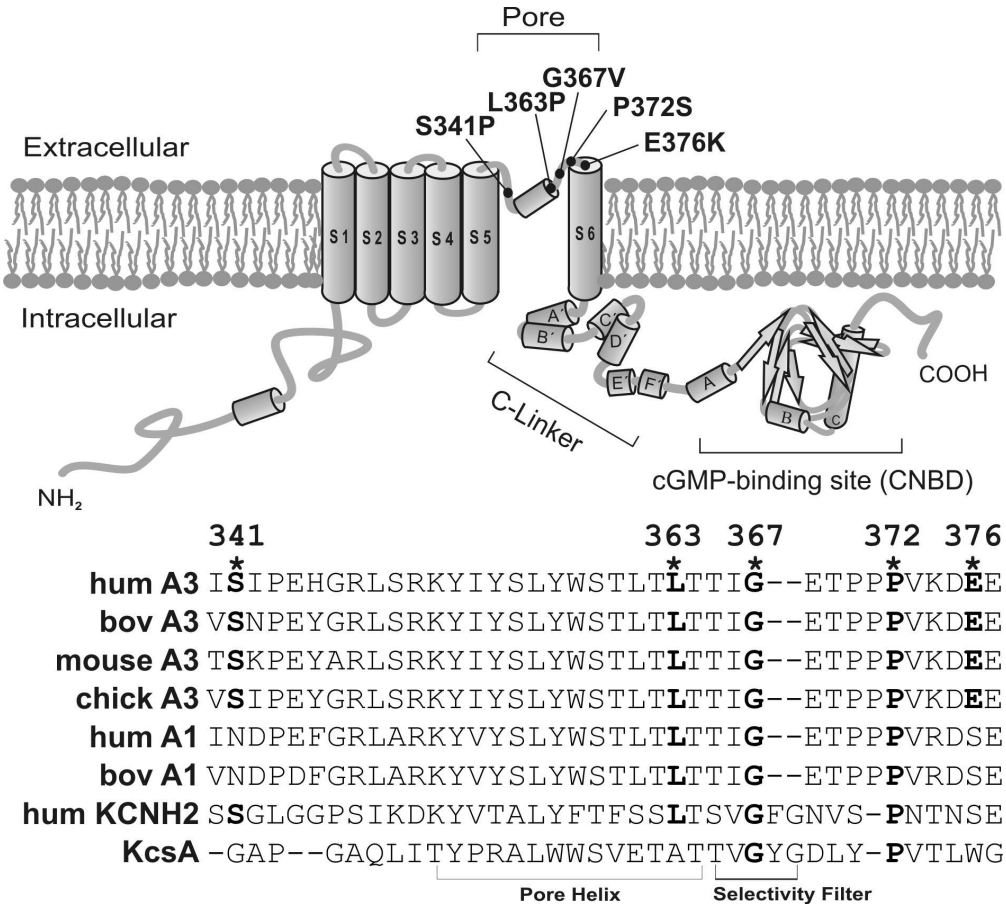

Figure 1. Structure of the CNGA3 subunit and sequence alignment of the pore region
The topological model of the CNGA3 polypeptide depicts six transmembrane helices (S1-S6), a pore region and a C-linker connecting pore region and cyclic nucleotide-binding site (CNBD). The analyzed mutations in the pore region of the channel are depicted at their respective positions within the polypeptide. New mutations identified in this study are L363P, G367V and E376K. The alignment of the pore region shows the high evolutionary conservation of the mutated amino acid residues. GenBank accession numbers: Homo sapiens CNGA3 NP_001298.1, Bos taurus CNGA3 NP_776704.1, Mus musculus CNGA3 NP_034048.1, Gallus gallus CNGA3 NP_990552.1, Homo sapiens CNGA1 NP_000078.2, Bos taurus CNGA1 NP_776703.1, Homo sapiens KCNH2 NP_742053.1 and Streptomyces coelicolor KcsA NP_631700.1.
159x143mm (300 x 300 DPI)

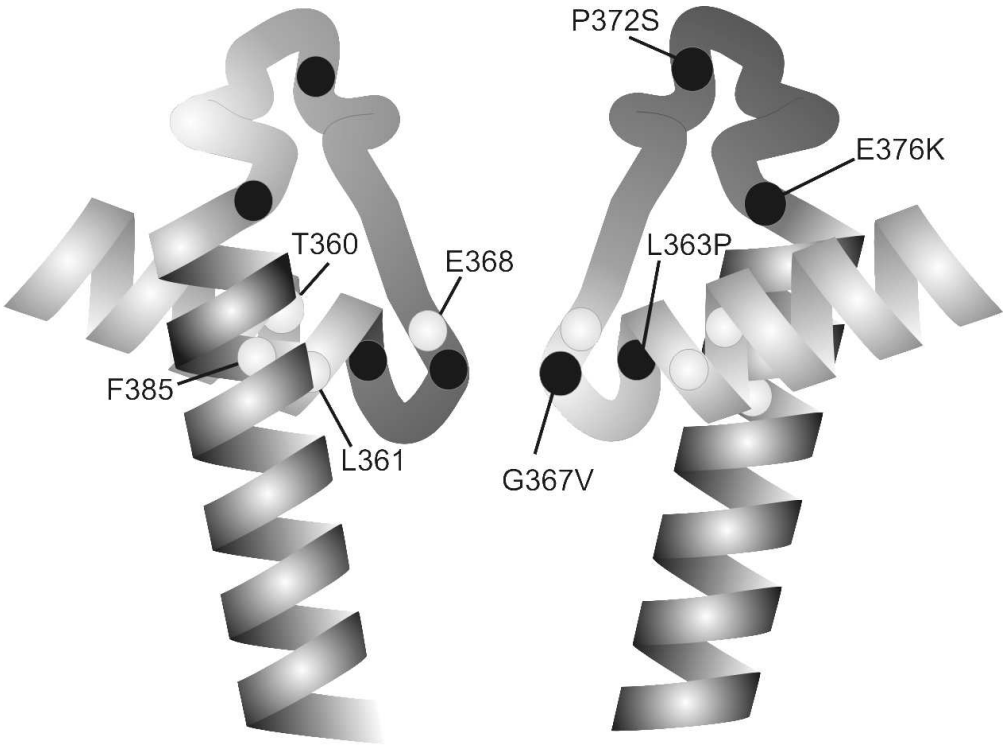

Figure 2. Schematic drawing of the pore-forming region of CNGA3. Depicted are two adjacent subunits and the locations of four of the analyzed mutations (black circles) as well as the positions of amino acid residues forming intrasubunit interactions (grey circles) within the pore region (Mazzolini, et al., 2009). Adapted from (Giorgetti, et al., 2005).
159x117mm (200 x 200 DPI)

For Review

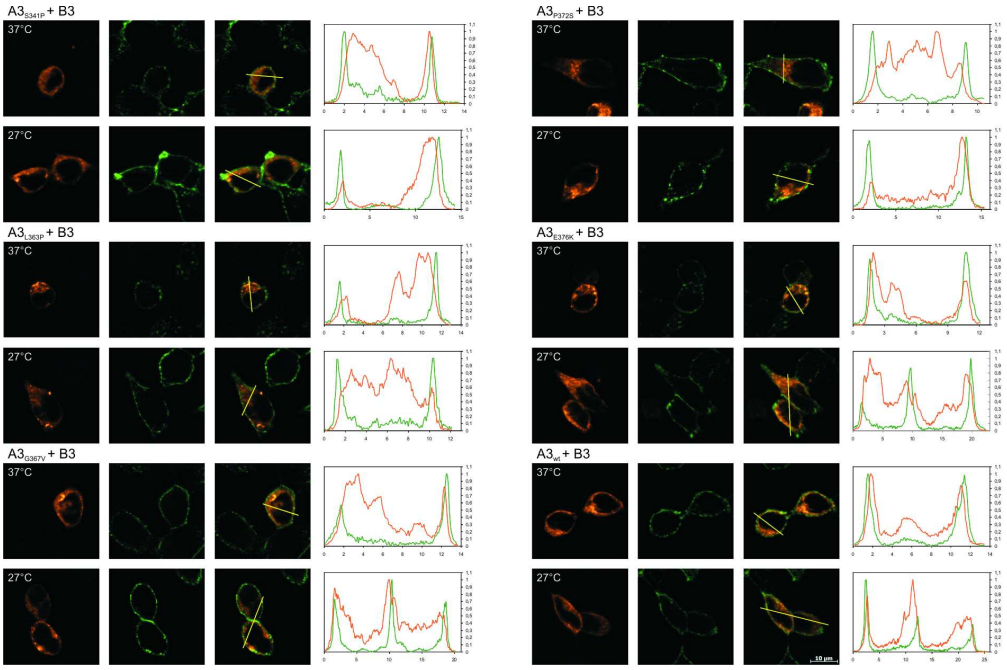

Figure 3. Analysis of the surface expression of wild-type and mutant A3 channels. HEK293 cells were transfected with wild-type or mutant A3 plus wild-type B3 and incubated at either 37°C (top row) or 27°C (bottom row) for >24 h. The left column shows A3 channels stained with an Alexa Fluor 660-coupled secondary antibody (orange). The cell membrane labeling with WGA-Alexa Fluor 488 is depicted in the center column (green). Overlays of the two stainings are shown in the right micrograph column. Yellow lines in the overlay pictures indicate the axis along which the fluorescence intensities of the two fluorophors were determined. Fluorescence intensities were measured through a slice at the center of the cells at a distance of 0.2-0.3 µm and normalized to the maximum fluorescence intensity. The normalized fluorescence intensities (y-axis) of WGA-Alexa Fluor 488 (green line) and Alexa Fluor 660 (orange line) are plotted against the distance (x-axis) in the adjacent diagrams. Like $A3_{wt}$ + B3, $A3_{E376K}$ + B3 co-localized with the plasma membrane after incubation of transfected HEK293 cells at either temperature. Surface expression of $A3_{G367V}$ + B3 was impaired at 37°C, but not significantly different from wild-type channels at 27°C. For $A3_{L363P}$ + B3 and $A3_{P372S}$ + B3, membrane co-localization was impaired at both temperatures, but incubation of transfected cells at lower temperature led to an improvement of surface expression. In contrast to that, reduced surface expression of $A3_{S341P}$ + B3 could not be enhanced by lowering the cultivation temperature. The results of the quantification and statistical analysis of this data are displayed in Supp. Table S2.
159x105mm (300 x 300 DPI)

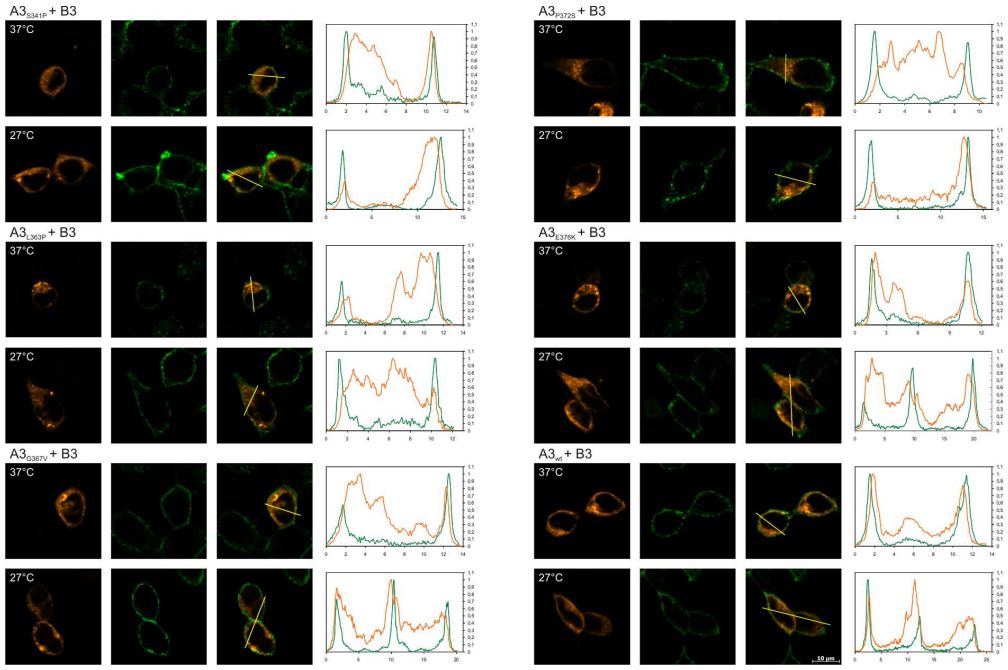

Figure 3 in RGB format
159x105mm (300 x 300 DPI)

Review

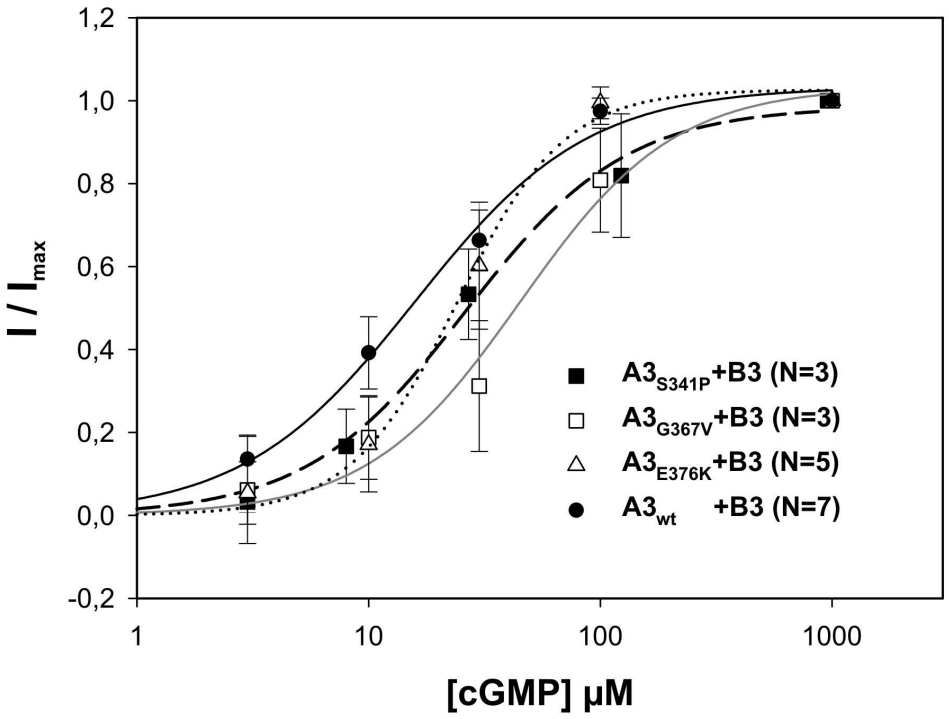

Figure 4. cGMP dose-response relationships of heteromeric channels.
Macroscopic potassium currents were recorded from inside-out patches of transfected HEK293 cells under symmetric ionic conditions. Currents evoked by different concentrations of cGMP at a membrane potential of +80 mV were normalized to the maximum current (with 1000 µM cGMP) after subtraction of leak currents. Normalized currents are plotted against log [cGMP] as arithmetic means ± SD. Statistical analysis using an unpaired t-test showed that the dose-response relationship of $A3_{G367V}$ + B3 is significantly different from that of wild-type channels (p = 0.006) while the other two mutants did not deviate significantly. The following $K_{1/2}$ values have been calculated using the Hill equation: $A3_{S341P}$ + B3 (dashed line) = 26 µM, $A3_{G367V}$ + B3 (grey line) = 45 µM, $A3_{E376K}$ + B3 (dotted line) = 24 µM and $A3_{wt}$ + B3 (black line) = 18 µM.
159x135mm (300 x 300 DPI)

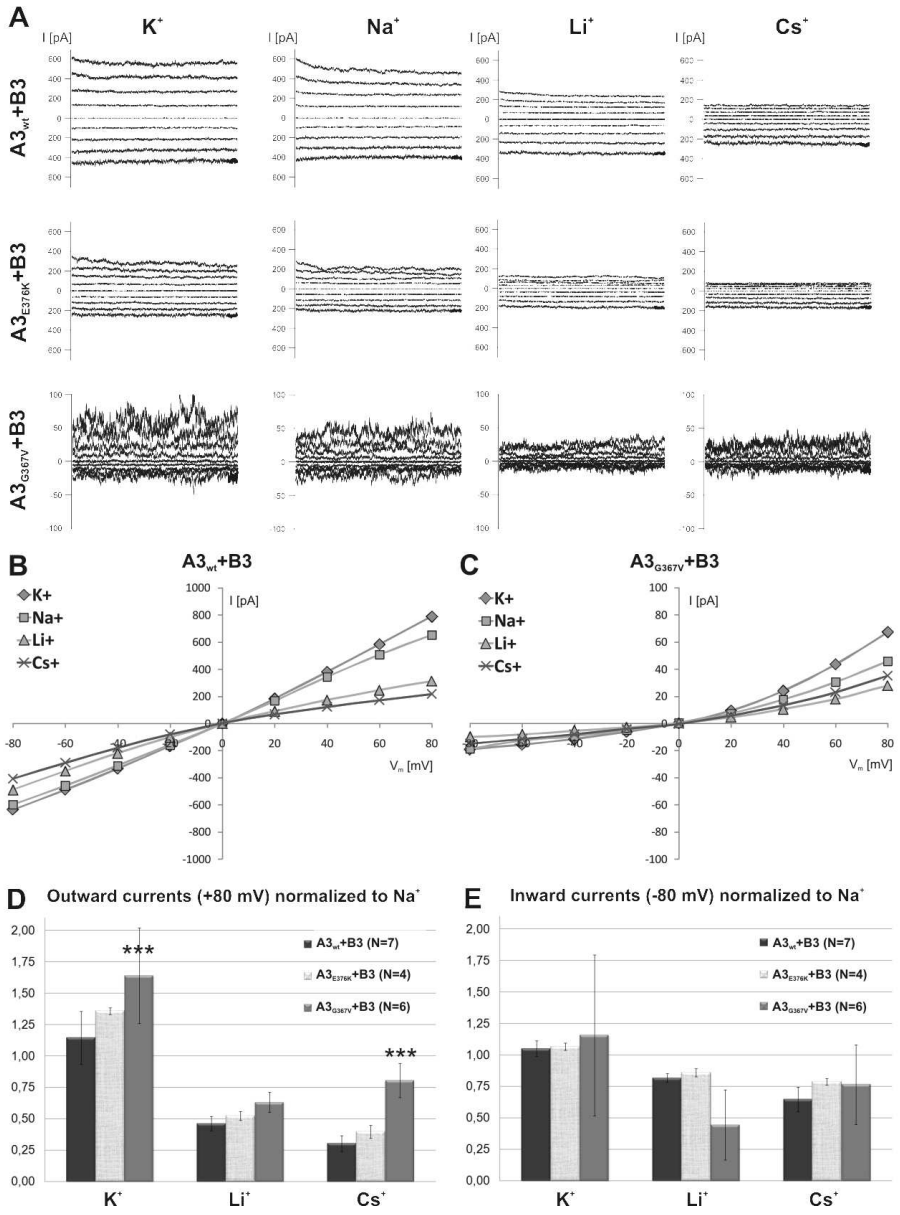

Figure 5. Selectivity for monovalent ions of pore mutants $A3_{E376K}$ + B3 and $A3_{G367V}$ + B3. (A) Representative traces of cGMP-evoked currents through wild-type or mutant channels for various monovalent ions. Current traces were recorded over a time of 300 ms at membrane potentials from +80 mV to -80 mV in 20 mV increments at a saturating cGMP concentration. (B + C) Representative I/V plots of wild-type and mutant heteromeric channels. Macroscopic currents for monovalent ions are plotted against the membrane potential. Ion selectivity of $A3_{E376K}$ + B3 was similar to the wild-type (B). $A3_{G367V}$ + B3 showed an outward rectification and markedly reduced macroscopic currents (C). The selectivity sequences for outward and inward currents are $I_K > I_{Na} >> I_{Li} > I_{Cs}$ for $A3_{wt}$ + B3 and $A3_{E376K}$ + B3, but $I_K > I_{Na} > I_{Cs} > I_{Li}$ for $A3_{G367V}$ + B3. Panels (D + E) show fractional currents of K^+, Li^+ and Cs^+ normalized to the Na^+ current at a membrane potential of +80 mV (D) and -80 mV (E). *** indicates statistically significant difference of $A3_{G367V}$ + B3 K^+ and Cs^+ permeability compared to wt as determined with two-way ANOVA ($p < 0.001$).

160x212mm (200 x 200 DPI)

For Peer Review

Table 1 Overview of patient genotypes and clinical findings

Family[#]	Diagnosis	Allel 1[#]	Allel 2[#]	Age at exam	Sex	Visual Acuity (OD/OS)	Cone ERG	Color Vision	Photophobia	Nystagmus
CHRO 119-8647*	iACHR	S341P	R223W	3	M	0.20/0.20	residual	abnormal	moderate	yes
CHRO 367-2641	cACHR	S341P	R277G	12	M	0.04/0.05	n.d.	none	yes	yes
CHRO 301-11168	ACHR	**L363P**	**L363P**	5	F	n.d.	n.d.	abnormal	yes	yes
CHRO 301-11169	ACHR	**L363P**	**L363P**	1	M	n.d.	residual	n.d.	n.d.	yes
CHRO 293-10826	cACHR	**G367V**	**G367V**	4	M	0.10/0.07	none	none	yes	yes
CHRO 293-10825	ACHR	**G367V**	**G367V**	2	F	n.d.	n.d.	n.d.	yes	yes
CHRO 356-12170	cACHR	**G367V**	**G367V**	12	M	0.10/0.10	no response	none	yes	yes
CHRO 389-13406	ACHR	**G367V**	**G367V**	29	M	n.d.	n.d.	n.d.	n.d.	n.d.
CHRO 121-8655*	ACHR	P372S	P372S	5	F	0.15/0.15	n.d.	none	yes	yes
CHRO 532-16588	cACHR	P372S	P372S	23	F	0.10/0.10	no response	none	yes	yes
CHRO 544-16904	ACHR	P372S	P372S	4	F	0.20/0.20	residual	abnormal	yes	yes
CHRO 124-8699*	cACHR	P372S	R283W	10	F	0.10/0.10	no response	none	yes	yes
CHRO 124-8700*	cACHR	P372S	R283W	11	M	0.10/0.10	no response	none	yes	yes
CHRO 383-12408	ACHR	**E376K**	**E376K**	6	M	0.10/0.10	n.d.	abnormal	yes	yes

[#] Newly reported patients and newly identified mutations are indicated in bold; *patients published previously by Wissinger et al., 2001. Abbreviations: ACHR = unclassified type of achromatopsia, cACHR = complete achromatopsia, iACHR = incomplete achromatopsia, n.d. = no data

For Peer Review

For Peer Review

Table 2 Results of calcium imaging experiments

CNGA3	Calcium imaging			
channel[#]	A3 37°C*	A3 27°C*	A3 + B3 37°C*	A3 + B3 27°C*
S341P	x	x	x	**33%**
L363P	x	x	x	x
G367V	x	x	x	**23 %**
P372S	x	x	x	x
E376K	x	x	x	**27 %**
wild-type	**69 %**	**100 %**	**65 %**	**96 %**

[#] Cells were co-transfected with wild-type or mutant CNGA3 expression constructs and a CFP plasmid and subsequently incubated at 37 °C or 27°C.

* Percentages refer to the fraction of CFP-positive cells that showed a calcium influx signal, x=no response

For Peer Review

Table 3 $K_{1/2}$ Values and Hill Coefficients (± SD) of the Activation of Heteromeric Channels by cGMP at a Membrane Potential of +80 mV

Channel	N	h	$K_{1/2}$ [µM cGMP]	p-value	shift of $K_{1/2}$
$A3_{wt}$ + B3	7	1.17 ± 0.12	17.96 ± 1.71	-	-
$A3_{S341P}$ + B3	3	1.26 ± 0.17	26.31 ± 3.65	0.0992 (n.s.)	→ 1.5x
$A3_{G367V}$ + B3	3	1.31 ± 0.28	45.34 ± 9.37	**0.006 (**)**	**→ 2.5x**
$A3_{E376K}$ + B3	5	1.88 ± 0.22	24.10 ± 1.77	0.1011 (n.s.)	→ 1.3x

p-values were determined with an unpaired t-test and indicate statistical significance of mutant data compared to the wt control. $p > 0.05$ was considered not significant (n.s.), $p < 0.01$ very significant (**).

Arrows indicate direction of shift of $K_{1/2}$ compared to the wild-type value.

N = number of patches, h = Hill coefficient, $K_{1/2}$ = ligand concentration of half-maximum activation

For Peer Review

Table 4 Permeability ratios (± SD) of wild-type and mutant channels for K^+, Li^+ and Cs^+ normalized to Na^+ currents = 1.

Channel	N	V_m	K^+	p	Li^+	p	Cs^+	p
$A3_{wt}$ + B3	7	+80 mV	1.14 ± 0.21	-	0.46 ± 0.06	-	0.30 ± 0.06	-
		- 80 mV	1.05 ± 0.06	-	0.82 ± 0.03	-	0.65 ± 0.10	-
$A3_{G367V}$ + B3	3	+80 mV	**1.64 ± 0.38*****	**< 0.001**	0.63 ± 0.08	> 0.05	**0.81 ± 0.13*****	**< 0.001**
		- 80 mV	1.15 ± 0.64	> 0.05	0.44 ± 0.28	> 0.05	0.77 ± 0.32	> 0.05
$A3_{E376K}$ + B3	5	+80 mV	1.36 ± 0.03	> 0.05	0.52 ± 0.04	> 0.05	0.40 ± 0.05	> 0.05
		- 80 mV	1.07 ± 0.03	> 0.05	0.86 ± 0.03	> 0.05	0.79 ± 0.02	> 0.05

p-values were determined with two-way ANOVA and indicate extent of statistically significant difference of mutant data compared to the wt control. $p > 0.05$ was considered not significant (n.s.), $p < 0.001$ extremely significant (***).

For Peer Review

Supplementary Material

SUPP. TABLE S1. New *CNGA3* Mutations Identified in Achromatopsia Patients

Exon	Mutation*	Amino acid substitution	Allelic state in patient	Family CHRO
7	c.1088T>C	p.L363P	Homozygous	301
7	c.1100G>T	p.G367V	Homozygous	293, 356, 389
7	c.1126G>A	p.E376K	Homozygous	383

*Nucleotide numbering reflects *CNGA3* cDNA numbering with +1 corresponding to the A of the ATG translation initiation codon in the reference sequence (NM_001298.2), according to journal guidelines (www.hgvs.org/mutnomen). The initiation codon is codon 1.

For Peer Review

SUPP. TABLE S2. Results of the co-localization analyses.*

Channel	N	Manders'overlap coefficient ± SD	37°C versus 27°C[a]	Presence of B3 subunit[b]	Wild-type versus mutant[c]
$A3_{wt}$ 27°C	12	0.56 ± 0.07	p < 0.001	-	-
$A3_{wt}$ 37°C	9	0.69 ± 0.04		-	-
$A3_{S341P}$ 27°C	11	0.47 ± 0.06	n.s.	-	p < 0.05
$A3_{S341P}$ 37°C	15	0.46 ± 0.12		-	p < 0.001
$A3_{L363P}$ 27°C	13	0.43 ± 0.07	n.s.	-	p < 0.001
$A3_{L363P}$ 37°C	12	0.38 ± 0.09		-	p < 0.001
$A3_{G367V}$ 27°C	12	0.44 ± 0.10	n.s.	-	p < 0.01
$A3_{G367V}$ 37°C	12	0.47 ± 0.08		-	p < 0.001
$A3_{P372S}$ 27°C	13	0.40 ± 0.07	n.s.	-	p < 0.001
$A3_{P372S}$ 37°C	16	0.37 ± 0.13		-	p < 0.001
$A3_{E376K}$ 27°C	11	0.42 ± 0.13	n.s.	-	p < 0.05
$A3_{E376K}$ 37°C	10	0.44 ± 0.06		-	p < 0.001
$A3_{wt}$ + B3 27°C	11	0.57 ± 0.08	n.s.	n.s.	-
$A3_{wt}$ + B3 37°C	13	0.59 ± 0.13		n.s.	-
$A3_{S341P}$ + B3 27°C	15	0.48 ± 0.06	n.s.	n.s.	p < 0.05
$A3_{S341P}$ + B3 37°C	10	0.49 ± 0.07		n.s.	p < 0.05
$A3_{L363P}$ + B3 27°C	12	0.36 ± 0.09	p < 0.05	n.s.	p < 0.001
$A3_{L363P}$ + B3 37°C	13	0.30 ± 0.06		p < 0.05	p < 0.001
$A3_{G367V}$ + B3 27°C	10	0.58 ± 0.08	n.s.	p < 0.01	n.s.
$A3_{G367V}$ + B3 37°C	10	0.47 ± 0.14		n.s.	p < 0.05
$A3_{P372S}$ + B3 27°C	17	0.46 ± 0.08	p < 0.001	p < 0.05	p < 0.05
$A3_{P372S}$ + B3 37°C	14	0.32 ± 0.09		n.s.	p < 0.001
$A3_{E376K}$ + B3 27°C	13	0.53 ± 0.06	n.s.	p < 0.05	n.s.
$A3_{E376K}$ + B3 37°C	11	0.52 ± 0.08		p < 0.05	n.s.

* To evaluate the incorporation of homomeric (only A3) and heteromeric (A3 + B3) into the plasma membrane of transfected HEK293 cells cultured at 27°C or 37°C the Manders' overlap coefficient (± SD) was calculated. N represents the number of analyzed cells. Statistical data analysis was performed using the Mann-Whitney rank sum test; n.s. = not significant.

[a] Evaluation of the effect of the cultivation temperature of transfected HEK293 cells onto the integration of mutant and wild-type channels into the plasma membrane.

[b] Statistical analyses of the impact of the presence of the B3 subunit onto the integration of wild-type and mutant channels into the plasma membrane.

[c] The incorporation of mutant homomeric and heteromeric channels into the cell membrane was compared to the analogous condition of wild-type channels.

For Peer Review

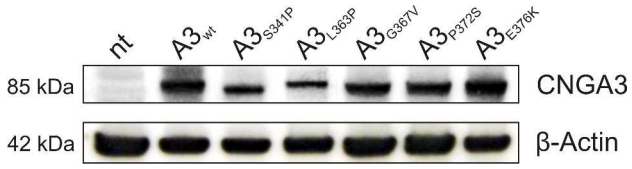

SUPP. FIGURE S1. Western blot with membrane fractions of cells expressing CNGA3 wild-type or mutant channels using anti-CNGA3 antibody SA3900 and β-actin as loading control. Untransfected cells (nt) were used as negative control.

For Peer Review

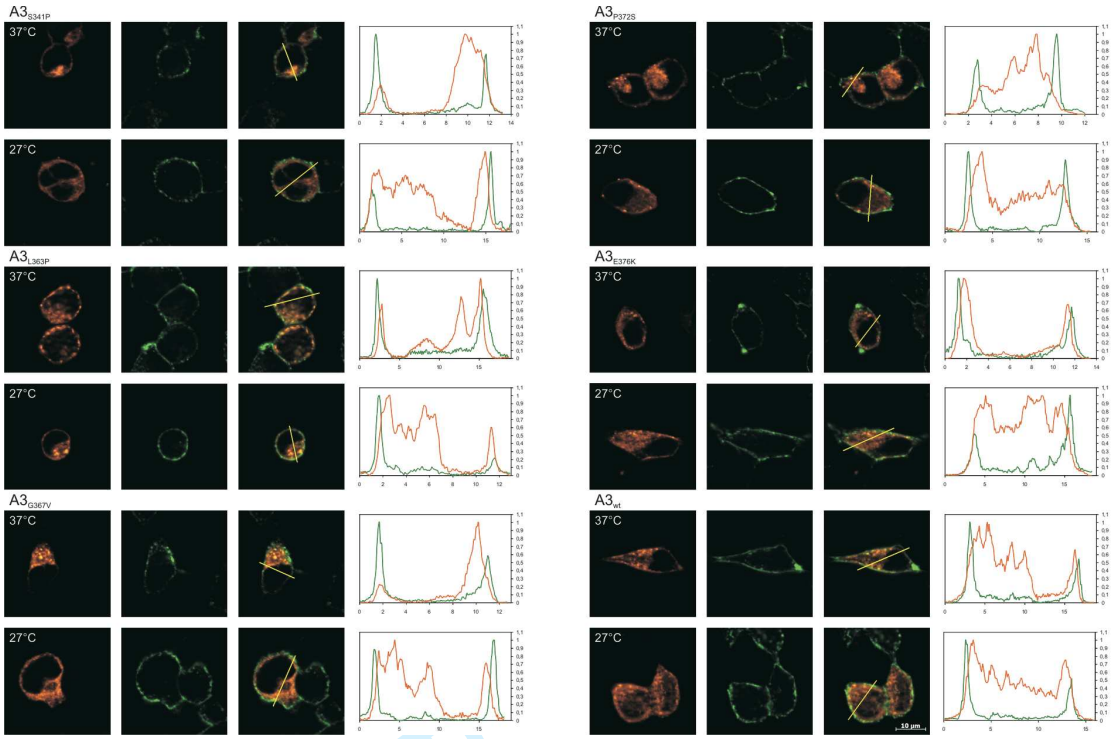

SUPP. FIGURE S2. Co-localization of homomeric wild-type and mutant CNG channels (orange) with the plasma membrane (green). Shown are immunocytochemical stainings of HEK293 cells expressing homomeric wild-type CNG channels or channels with the mutations S341P, L363P, G367V, P372S and E376K following incubation at 27°C or 37°C. All mutant channels showed impaired surface expression compared with the wild-type channel at both temperatures (compare Supp. Table S2).

Peer Review

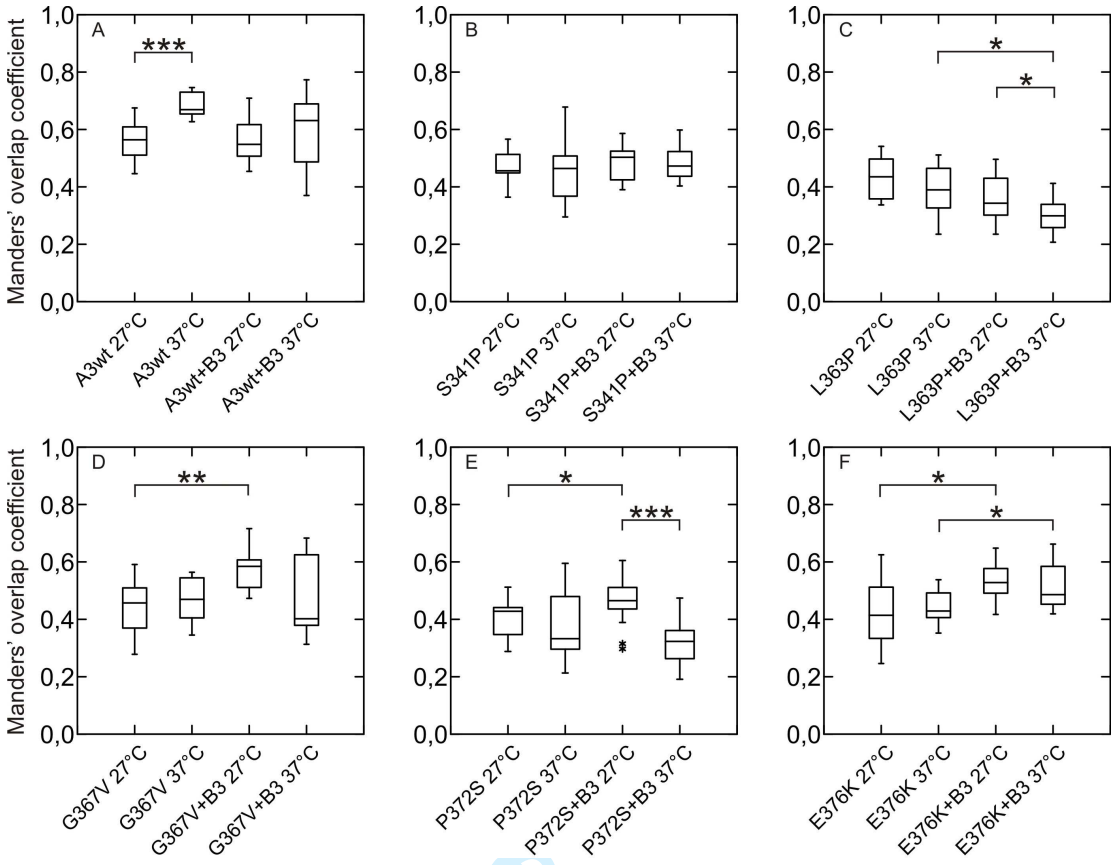

SUPP. FIGURE S3. Comparison of the integration of wild-type and mutant CNG channels into the plasma membrane in the absence or presence of the B3 subunit and after incubation of transfected cells at 27°C or 37°C.

The Manders' overlap coefficients were calculated to quantify the integration of CNG channels into the plasma membrane of transfected HEK293 cells. Calculated values for homomeric and heteromeric wild-type channels (A) and channels with the mutation S341P (B), L363P (C), G367V (D), P372S (E) and E376K (F) are shown as box plots. At least 9 cells were analyzed for each condition. Statistical data analysis was performed using the Mann-Whitney rank sum test. $p > 0.05$ was considered not significant, $p \leq 0.05$ was considered significant (*), $p \leq 0.01$ very significant (**) and $p \leq 0.001$ extremely significant (***).

er Review

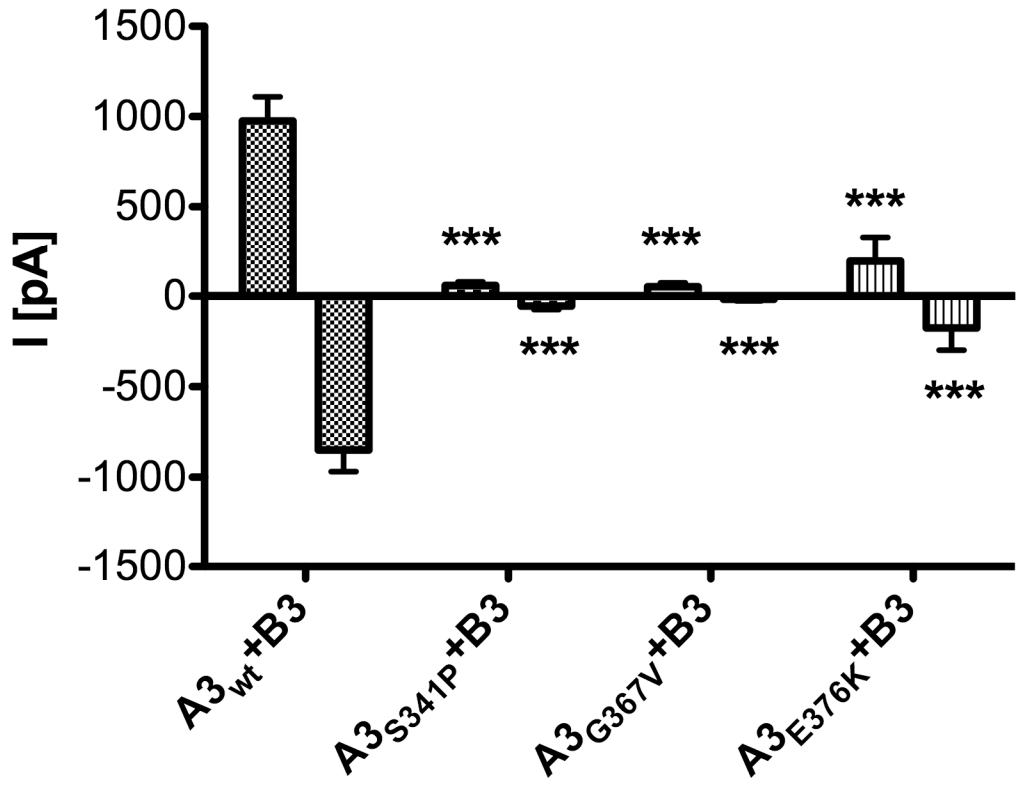

SUPP. FIGURE S4. Mean maximum currents ± SD of wild-type and mutant channels at +80 mV and -80 mV in the presence of 1000 µM cGMP. Mean currents were 976 ± 354 pA (+80 mV) and -850 ± 314 pA (-80 mV) for $A3_{wt}$ + B3, 60 ± 34 pA (+80 mV) and -54 ± 34 pA (-80 mV) for $A3_{S341P}$ + B3, 46 ± 29 pA (+80 mV) and -19 ± 11 pA (-80 mV) for $A3_{G367V}$ + B3 and 195 ± 304 pA (+80 mV) and -175 ± 276 pA (-80 mV) for $A3_{E376K}$ + B3. ***The maximum cGMP-evoked currents of all mutant channels were significantly reduced compared to wild-type channels as determined by two-way ANOVA ($p < 0.001$).

For Review